# OPTIMIZATION OF ARTILLERY PROJECTILES BASE DRAG REDUCTION USING HOT BASE FLOW

***Mohammed Amin DALI*[*1], *Slobodan JARAMAZ*[2]**

[*1] University of Defence, Military Academy, Belgrade, Serbia

[2] University of Belgrade,Faculty of Mechanical Engineering,Belgrade, Serbia

[*] Corresponding author; E-mail: DaliMA380@gmail.com

*The computational fluid dynamics (CFD) numerical simulations were carried out to investigate the base drag characteristics of a projectile with base bleed unit with a central jet. Different base bleed grain types with differnet combustion temperatures were used. The goal was to find a way to effectively control the base flow for base drag reduction and optimisate the latter using an adequate (CFD) software. Axisymmetric, compressible, mass-averaged Navier-Stokes equations are solved using the k-ω SST, transition k-kl-ω and RSM turbulence models. The various base flow characteristics are obtained by the change in the non-dimensionalized injection impulse. The results obtained through the present study show that there is an optimum bleed condition for all base bleed grains tested. That optimum is dependent on the temperature of the grain combustion products. The optimum reduces the total drag for 6,9% in the case of air injection at tempreture of 300K and reaches up to 28% in the case of propellant combustion products injection at almost 2500K. Besides, the increasing of molecular wight has a role no less important than temperature of the combustion products in terms of base drag reduction.*

Key words*: artillery projectiles, base bleed, drag reduction, CFD, combustion temperature*

## 1. Introduction

The extended firing ranges and impact precisions of weapons systems are expected to be constantly improved; especially when new ammunition is developed or when existing ammunition is modified. Aerodynamic bodies such as projectiles, missiles, and rockets generally, undergo deterioration of flight performance by drag. The total drag for projectiles can be divided into three components: (1) pressure drag (excluding the base), (2) viscous (skin friction) drag, and (3) base drag[1]. Notably, among the three components of the drag affecting a projectile, the base drag frequently accounts for one-half, or even much more, of the total drag for large caliber ammunitions. Reducing the base drag is an efficient and practical way to reduce the total drag of projectile [2], and increase the range of projectile for up to 30%. Afterbody boattailing, base bleed or base burning, some vortex suppression devices and their combinations can achieve base drag reduction. Such active or passive flow control techniques, basically, manipulate or alter the near-wake flowfield for an increase in base pressure and consequently reduce base drag [3]. In [4] have been proven that the peak average base pressure ratio ($P_b/P_\infty$) at optimal impuls is 18.5% higher than the average base pressure ratio of the blunt based cylinder and 5.7% higher than

that of the boattailed afterbody. The base bleed technology is particular effective for long-range flights, where the integrated effect of the drag reduction is manifested. Such a capability is of significant current interest. Detailed understanding of the energy as well as mass addition and the fluid-dynamic interactions occurring around the projectile and especially the afterbody flow is a requirement before proposing solutions to reduce the drag [5, 6]. In actual system, the mass flow rate injected in the afterbody flow is provided by the combustion of the propellant. The base pressure of a projectile traveling at supersonic speed can be controlled by burning this propellant near the base region. Experiments performed by several researchers [6-9] to study the effect of bleed mass flow rate on the base pressure exhibit certain common characteristics and indicate three distinct operating regimes based on the quantity of bleed fluid injected. The results of various studies using air, hydrogen, helium, argon and nitrogen have shown that afterbody flows with base bleed can result in base drag reduction [6-9]. The significant increases in base pressure have also been observed using a heated bleed gas [6, 9]. At low injection rates, the base pressure rise is nearly proportional to the enthalpy of the bleed gas. The peak base pressure is higher, and occurs at a lower of the bleed mass flow rate, than for the corresponding cold bleed case [6, 9]. Therefore, present study is focused on base drag optimization of a 122 mm artillery projectiles using a base bleed technology. The drag reduction estimation was determined performing several CFD calculations. During the different numerical simulations, the effect of propellant grain composition and temperature of different combustion products were discussed together with temperature influence of some pure gases. Also, we study the influence of air temperature on base drag due to our further intention to investigate effect of air temperature in wind tunel.

## 2. Computational approach

The (2-D) axisymmetric body projectiles configurations are considered in this paper due to the physical complexity of the entire process. The base flow field is described with the Reynolds Averaged Navier-Stokes (RANS) computational fluid dynamics software (CFD) [10-13]. Using three turbulence models k-ω SST (The shear stress transport) (2 equations) [13], transition k-kl-ω (3 equations) and Reynolds Stress Model RSM (5 equations), are used (default constant values were employed for these models) [2, 11]. These models were tested and compared with the semi-empirical engeneering model (ADK0) using aerodynamic prediction based on [13] theories. In addition, these results were compared with experimental results obtained by 3D radar in the case of standard projectile. The equations considered in this study for a compressible fluid flow behind projectile base are [11, 14, 15].

Continuity
$$\frac{\partial \rho}{\partial t}+\frac{\partial(\rho u_i)}{\partial x_i}=0 \tag{1}$$

Momentum
$$\frac{\partial(\rho u_i)}{\partial t}+\frac{\partial(\rho u_i u_j)}{\partial x_j}=-\frac{\partial P}{\partial x_i}+\frac{\partial}{\partial x_i}\tau_{ij} \tag{2}$$

Energy
$$\frac{\partial}{\partial t}[\rho(e+\frac{V^2}{2})]+\frac{\partial}{\partial x_j}[\rho u_j\left(e+\frac{V^2}{2}\right)+P+q_j-u_i\tau_{ij}\ ]=0 \tag{3}$$

Note that, u denotes instantaneous velocity, V velocity modulus, ρ gas density, P gas pressure, $q_j$ heat flux and $\tau_{ij}$ viscous stress tensor. In addition, the perfect gas equation of state was considered. For the closure of the system, three turbulence models are used [11, 15-17].

According to [3], the Reynolds Stress Model *RSM* gave good results compared to experimental results, The *RSM* model is used in the most of this study, especially in sections **3.2** and **3.**

### 2.1. Hypothesis and boundary conditions

The characteristic time of variation of the boundary conditions was considered bigger than the characteristic residence time of the fluid particle within the domain. This means that the transient terms in the mass, momentum, and energy conservation equations were negligible compared to the convective terms. Therefore, the simulations were performed considering steady state boundary conditions for different flight conditions. The atmospheric conditions, considered as stagnation conditions. This way, different flight conditions cases were simulated to obtain the body drag coefficient at different Mach numbers, and different mass flux injection. The fluid considered in the simulations was air and propellant combustion gases. For both gases, the ideal gas assumption was used. The constant values were assumed for heat capacities. The Sutherland law for variable dynamic viscosity was used due to the high temperature ranges encountered in the problem studied. The projectiles were assumed to fly under zero angle of attack. All the walls were considered adiabatic. The flow field was considered compressible and the far field conditions were imposed at the external boundary, where the flight Mach number, pressure and temperature (stagnation values) were introduced. The entire domain was initialized with these far field conditions [15]. The projectile body was modelled as axisymmetric. The grid was generated using the appropriate mesh generator. The numerical structured discretization of the computational domain around the model was done with quadrilateral cells with ($y^+$~1) on the wall. The mesh number of the grid is almost 300000 cells (600 cells were used on the projectile, a 100 of them were used at the base) (see Fig. 1 left). This grid density was determined after tested several grid density types (see Fig. 1 right).

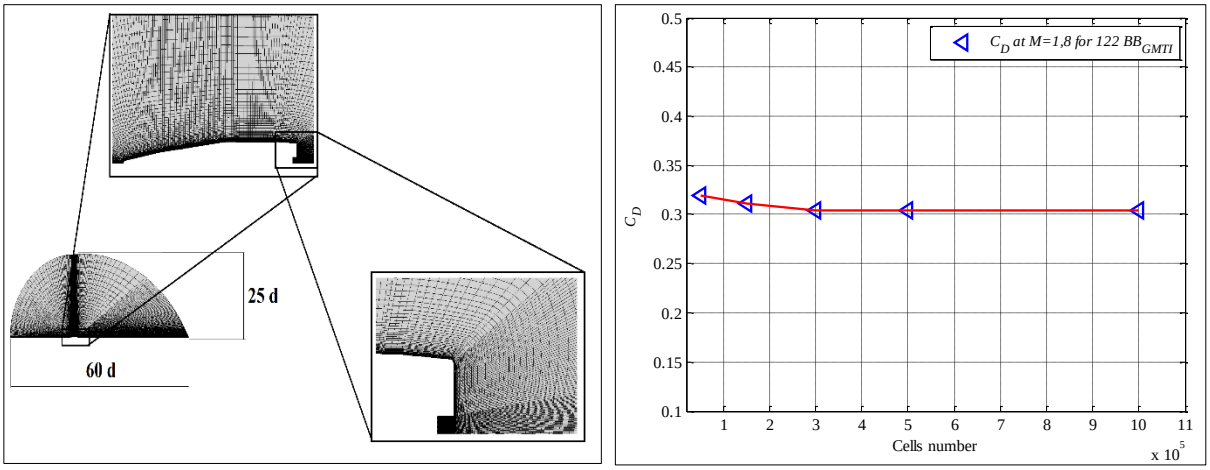


**Figure 1. Grid domain, grid near model and grid near base (Left- d is the caliber of projectile), $C_D$ vs cells number (Right)**

Regarding the propellant combustion at the Base Bleed unit, a simple approach was considered; the combustion process was modelled as normal injecting of gas mass flow rate at a fixed temperature through the orifice. The temperature and mass flow rate values were obtained from the propellant combustion data. The relative chamber pressure was estimated from the static experimental combustion tests. The thermodynamic parameters and the composition of combustion products are introduced. They were obtained with the help of the thermochemical calculation (TERMO code), which is developed

based on [18]. Different types of propellants are used in this study. In the Tab. 1 is shown the species used in the CFD simulation for every propellant:

**Table 1. The molar fractions of main species generated during the base bleed**

| Propellant | Molar fraction of | | | | | | Temperature of the products of combustion (K) | ΔQ (kJ/Kg) |
|---|---|---|---|---|---|---|---|---|
| | $CO_2$ | CO | $H_2O$ | $H_2$ | $N_2$ | HCl | | |
| GMTI | 3.045e-2 | 3.271e-1 | 1.131e-1 | 3.427e-1 | 6.361e-2 | 1.225e-1 | 1731 | -2272.1 |
| GST_1 | 4.704e-2 | 2.724e-1 | 2.295e-1 | 2.288e-1 | 7.407e-2 | 1.481e-1 | 2287 | -5301.3 |
| GST_2 | 7.617e-2 | 8.116e-2 | 4.946e-1 | 1.060e-1 | 2.421e-1 | 0.000 | 2050 | -7295.6 |
| GAL | 1.896e-2 | 2.152e-1 | 1.906e-1 | 3.780e-1 | 1.975e-1 | 0.000 | 2262 | -7293.8 |
| GHO | 8.890e-2 | 4.445e-1 | 1.904e-1 | 1.526e-1 | 1.232e-1 | 0.000 | 2442 | -1971.5 |
| GPVC | 4.565e-2 | 2.681e-1 | 2.223e-1 | 1.965e-1 | 6.876e-2 | 1.982e-1 | 2587 | -4970.2 |

The first propellant (known as GMTI) is the most used propellant in the base bleed unit. It is based on ammonium perchlorate (AP), hydroxyl-terminated polybutadiene (HTPB), ferric oxide ($Fe_2O_3$ – used as a combustion regulator (the lowest combustion temperature)) and additives. The second GST_1 is a mixture in which are crystalline AP/HTPB and additives [19]. Besides, the GST_2 samples consist of ammonium nitrate (AN), HTPB and minority additives. The GAL propellant is made of aluminized AP / HTPB mixture and some additives. The GHO is a homogeneous propellant mainly which contains the nitrocellulose (NC), the nitroglycerin (NGL), a small fraction of the dinitrotoluene (DNT) and the centralite I (C1) and some additives. Finally, the GPVC is a composite propellant which contains the ammonium perchlorate (AP), polyvinyl chloride (PVC), dioctyl-phthalate (DOP) and additives. In addition, in order to optimize base bleed composition, some preliminary simulations were performed with injection of Air, CO, $H_2O$ and HCl at different temperatures. All the base bleed grains were of the cylindrical shape with three segments. The external surface and one base of this cylinder were inhibited, and all of the internal surfaces and one base were non-inhibited (see Fig. 2).


**Figure 2. The GMTI base bleed grain used in this study**

### 2.2. The pressure of combustion products at the outlet of the orifice

Because the approach we considered is based on the injection of a gas mass flow rate and neglects the flow field in the Base Bleed cavity, the CFD simulation needs the introduction of the Supersonic/Initial Gauge Pressure. This notion specifies that overpressure value at the orifice outlet relative to the base pressure. This pressure can be obtained from the static experimental combustion tests. The results of this test are shown in Fig. 3

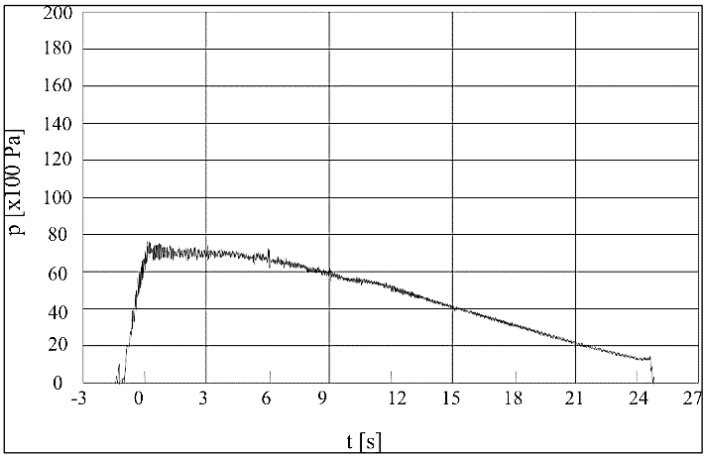


**Figure 3. The obtained results from the static experimental combustion test**

In our study, this test resulted in a chamber gauge pressure profile with a values of overpressure from zero to almost 75 mbar (see Fig. 3) for all propellants types. Therefore, in all CFD simulations related to the base bleed projectiles, we used an average value of 6000 Pa as a Supersonic/Initial Gauge Pressure.

### 2.3. Simulations overview

The computations were performed using the general-purpose software ANSYS-FLUENT™. The whole set of equations were solved by using an implicit pressure based solver with a second order upwind discretization scheme, Least Squares cell based method for gradient calculations and ROE-Flux-Difference Splitting flux evaluation schemes (ROE-FDS) [12, 15]. ROE-FDS scheme has shown to give good results when dealing with compressible flow problems.Pressure in the base bleed chamber and operating regimes

Fig. 4 illustrates the significant difference between the work principles of a base-bleed unit and a rocket motor[2-6, 15, 20-22]. This clearly demonstrates how the base pressure is affected by the injection mass flow rate. As the base-bleed propellant burns mainly under lower pressure, it is very important to study the combustion mechanism and properties under free ambient pressure [6, 20-22].

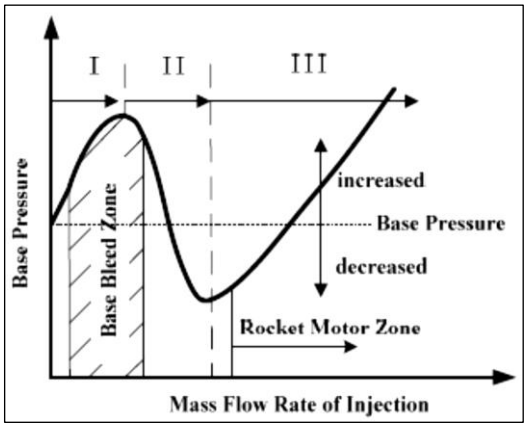


**Figure 4. Base pressure vs mass flow rate and the effect regime on base bleed**

The impulse $I$ is given by equation [20]:

$$I = \frac{\overset{g}{m}_g}{\overset{g}{m}_b} = \frac{r\, A_g\, \rho_g}{v_\infty\, A_b\, \rho_\infty} \qquad (4)$$

where r is the grain burn rate, $A_g$ is the burnt surface, $\rho_g$ is density of burning products, $V_\infty$ is projectile velocity, $A_b$ is base surface of the projectile and $\rho_\infty$ is air density.

In our case (base bleed grain combustion), we attempted to obtain the general burning-rate expression using the reported data based on the Saint Robert–Vieille law, which is often used to describe the burning rate over limited pressure ranges [22]

$$r = b g P_g^n \quad (5)$$

$P_g$ is the pressure, $n$ is the burning-rate pressure exponent, and $b$ is the constant of proportionality.

The pressure in the base bleed chamber is defined using the equality of mass flux of burning products through the orifice and mass flux of gas formed due to the grain burning. For the desired subsonic flow the following inequality should be satisfied. [20]

$$\frac{P_d}{P_g} > \left(\frac{2}{k+1}\right)^{\left(\frac{k}{k-1}\right)} \quad (6)$$

Where $P_d$ is projectile base pressure, $P_g$ is pressure in base bleed and k is specific heat ratio of burning products.

As given in [6], the effect of bleed mass flow rate on the base pressure exhibit certain common characteristics and indicate three distinct operating regimes based on the quantity of bleed fluid injected. At low values of bleed mass flow rate (regime I), the base pressure ratio increases fairly linearly with bleed rate. A peak in the base pressure ratio is observed at an intermediate value of bleed mass flow rate. Increases in base pressure ratio (relative to the no-bleed case) from 10 to 90% have been reported for the optimum bleed condition, which depends on factors such as the freestream Mach number and the size and geometry of the bleed orifice. Past the optimum value (regime II), the base pressure ratio decreases with increasing bleed rate until it reaches a relative minimum. Further increase in the bleed flow leads to an increase in base pressure ratio (regime III) due to the onset of power-on flow conditions.

## 3. Numerical tests and experimental investigation

In the study, the 3D radar type WEIBEL Doppler radar MFTR-2100 (The Multi Frequency Trajectory Radar system) is used to determine the drag force coefficient [23]. The howitzer 122mm D-30 artillery gun fired the standard and base bleed projectiles type. For every type of projectile two sets of five projectiles were fired at an elevation angle equal to $\theta_0 = 14{,}22°$.

### 3.1. Experimental validation

In order to illustrate the role of base bleed unit in the drag force coefficient reduction, two dimensional axisymmetric (2-D) numerical computations have been performed for the projectile configuration with jet interaction using ANSYS-FLUENT™ software at a different Mach numbers (from M = 0,4 to 2,2) corresponding to the projectiles Mach numbers flight .

Results were discussed in light of benchmarks between model predictions and experimental data (obtained from radar) and the results obtained from the semi-empiric ADK0 code [13]. The different drag coefficient results given by the CFD simulations (with therre turbulence models) were done [12]. For Mach numbers between 1 and 2.1, which is the velocity domain for projectiles with the base bleed working, there is a drag reduction up to 21% compared to the standard projectile. This confirms the efficiency of the base bleed unit in terms of extending the range of artillery projectile. In Fig. 5 (left), the experimental drag coefficient results (black squares) captured by the 3-D radar for the standard projectile is compared with the mean drag coefficient CFD results (to make it easier to see the results

better) for every projectile (green stars shape for standard projectile and red diamond shap for projectile with base bleed) and semi-empirical results (given by ADK0 code presented in figure by blue circle).It can be clearly seen there is a small shift between the CFD and the experimental drag coefficient results. The shift between the CFD and the experimental drag coefficient results is the consequence of the noise in the radar signals, which increases the error of real velocity measurements on the one hand [11, 23], and on the other hand the inherent in the CFD solutions performed with these computer codes is error or uncertainty in the results. These inherent inaccuracies are due solely to the fact that we are approximating a continuous system by a finite length, discrete approximation [24].(see Fig.5 (right)).

In the case of projectile with base bleed (122_BB) the capture was unsuccessful because of the long distance between the radar and the canon muzzle (This projectile is still in the development phase; hence, this distance was chosen as a safety precaution).

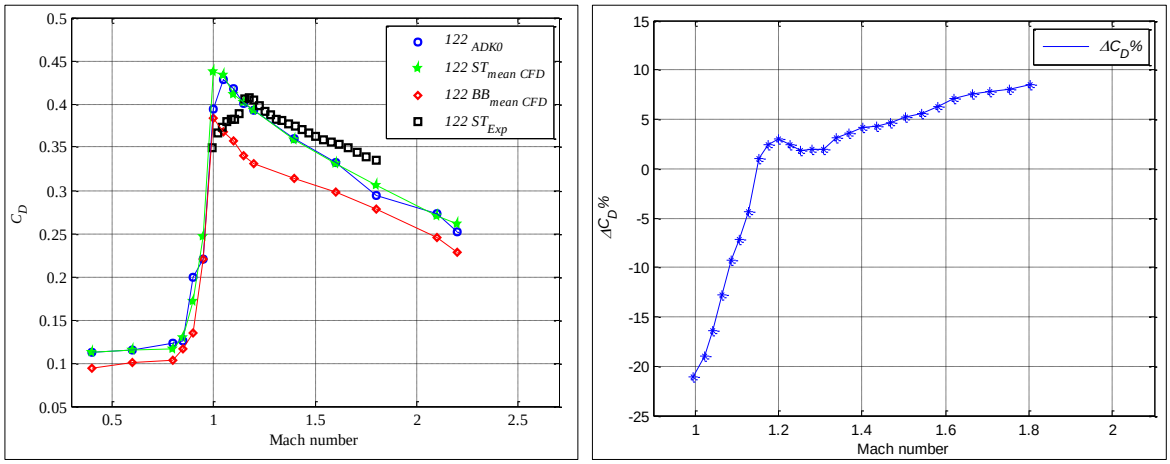


**Figure 5. The experimental $C_D$ vs M for the standard projectile compared to the mean CFD for each projectile and ADK0 results (Left), the relative error of CFD results related to the experimental result vs M (Right)**

### 3.2. The effect of the combustion temperature

Some researches as [3] have consided that the base bleed flow as an isoenergetic flow rate injected into the base region. But in reality, the injection mass flow rate is not at the same thermodynamic state as the thermodynamic state of the free stream air. Therefore the influence of the gas injection temperature (or gas injection enthalpy) into the wake region must be considered.

Many researches prove that base bleed units are more efficient when the flow field is supersonic type (Mach number > 1) [3, 5, 10, 15, 22, 25]. In this part of study, (2-D) numerical computations (CFD) have performed using ANSYS-FLUENT$^{TM}$ software at a different Mach numbers (from M = 0,9 to 2,2) and RSM model, for jet-on conditions (air at 300, 1700 and 2500 K and compared them with GMTI grain products at 1700 and 2500 K). In Fig. 6 is shown the CFD drag coefficient reduction results related to the standard projectile drag coefficient values, as a function of injected impulse (mass flow rate) for the projectile with air injection at different temperatures: 300K (left), 1700K (right) and 2500 K (down).

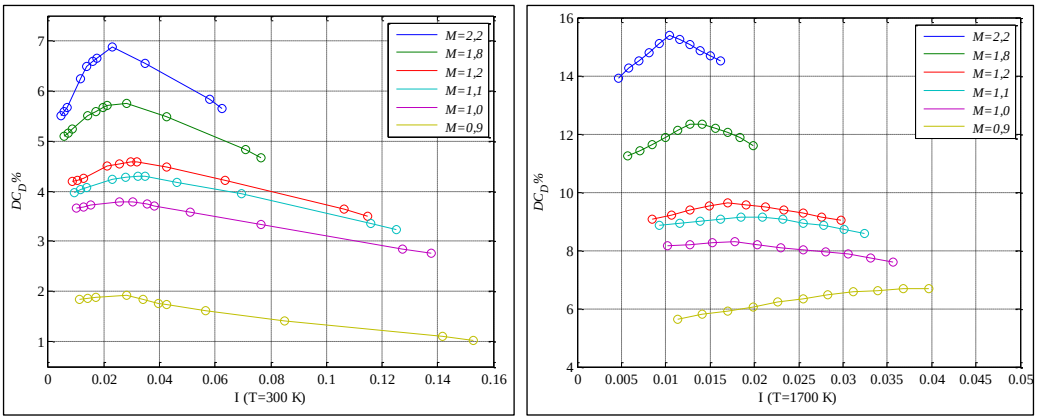


**Air injection (300K – Left) and Air injection (1700K-Right)**

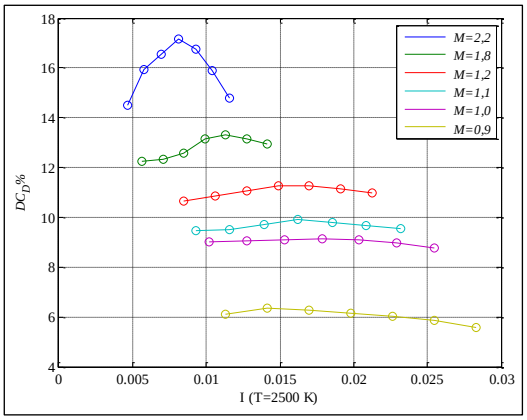


**Air injection (2500K)**

**Figure 6. Drag coefficient reduction vs injected impulse (mass flow rate) for the projectile with air injection**

From the Fig. 6, we can see that the drag coefficient reduction results ($\Delta C_D$ %) increase for the same Mach number with the increasing of temperature (at Mach number = 2,2 $\Delta C_D$ increases from ~7% at 300K to ~ 18% at 2500K). But the critical impulse ($I_{critical}$ is the highest value of the impulse after which there is not a drag reduction) decreases (from ~0,065 at 300K to ~0,012 at 2500K at Mach flight number = 2,2).

Fig. 7 shows the CFD drag coefficient reduction vs injected impulse (mass flow rate) for the projectile with GMTI combustion products injection at (a) 1731 K and (b) 2500 K using the RSM model.

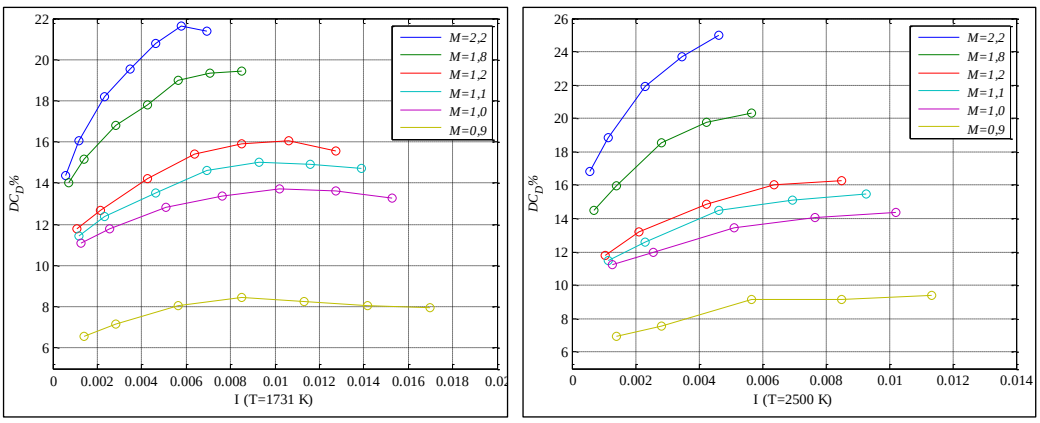


**Figure 7. Drag coefficient reduction vs injected impulse (mass flow rate) for the projectile with GMTI combustion products injection at 1731K (Left) and 2500 K (Right)**

As shown in Fig.7, the same can be observed with the injection of GMTI combustion products when the temperature changes from 1731K to 2500K. But in this case, the drag coefficient reduction results changes from 22% at 1731K to up to 26% at 2500K, at Mach flight number equal to 2,2. In addition, as shown in Fig.6 and Fig.7, we can confirm the good effect of the inceasing of the drag coefficient reduction caused by temperature of injected gas. Beside that, it is clear that at the same temperatures and for the same parametres (Mach number and impulse), the drag reduction results are greater for the projectiles with the GMTI combustion products injection than the one with air injection. This can be justified by the difference in nature of each fluid and probably the difference in the molecular weight.

In Fig. 8 are shown the base flow regions represented by the temperature distributions and streamline velocities (above) and the distributions of temperature (below) for each case with injection of the optimal impulse.

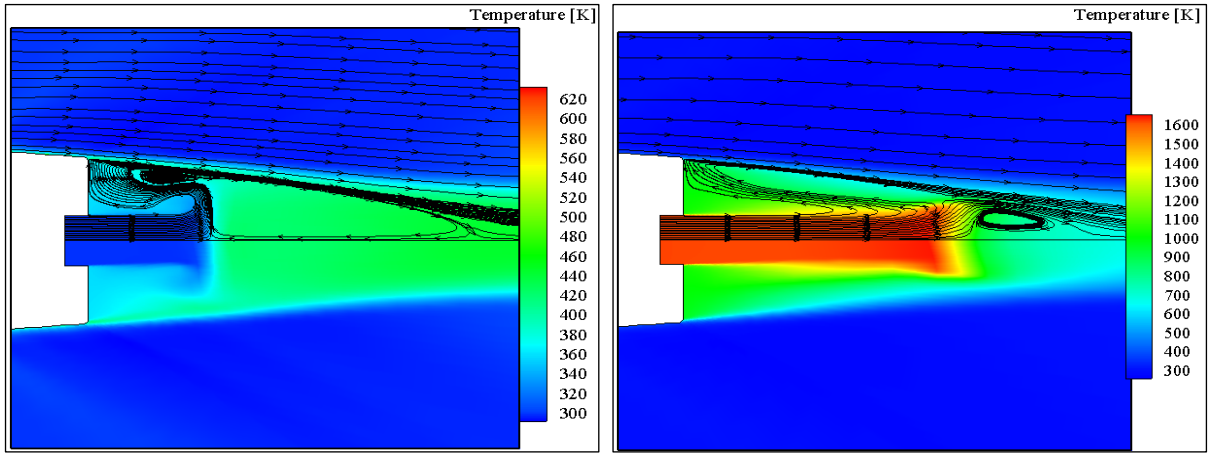


**Air (300K – Left) and Air (1700K – Right)**

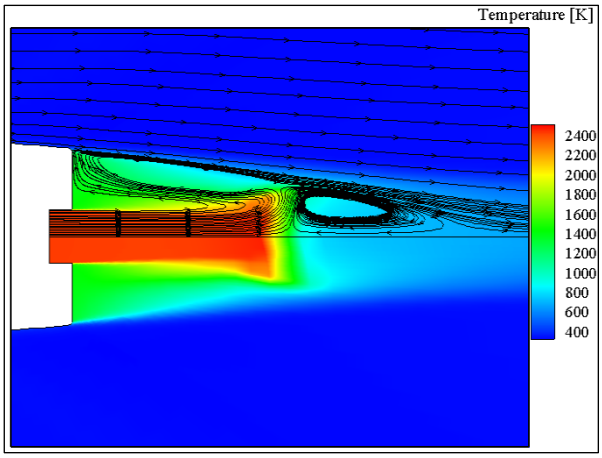


**Air (2500K)**

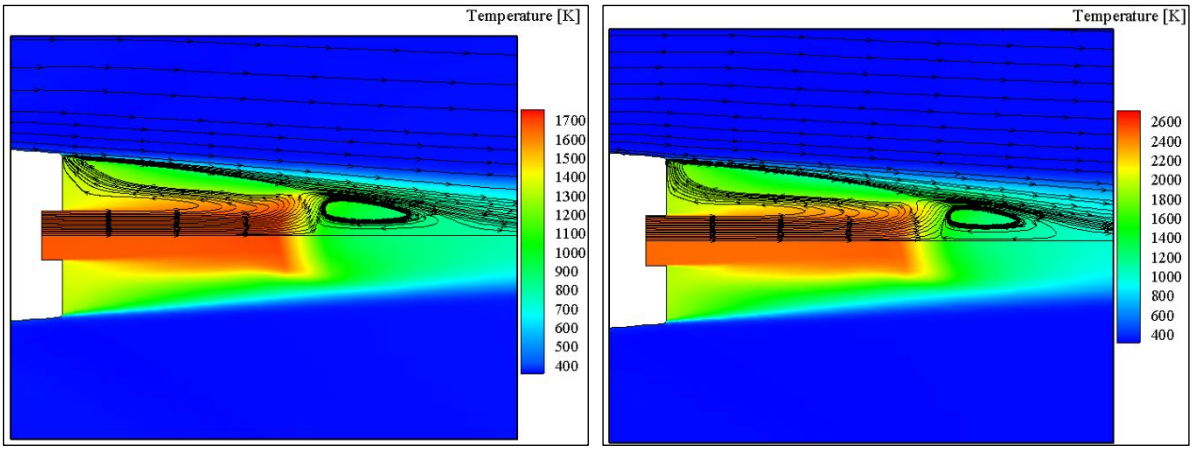


**GMTI (1731K – Left) and GMTI (2500K – Right)**

**Figure 8. Base flow regions represented by the streamline velocities and temperature distributions (up) and the temperature profiles (down) for each case with injection of the optimal impulse**

During the projectile flight, the reverse flow appears directly behind the projectile. The large turning angle behind the base causes separation and formation of reverse flow known as the recirculation region or the separation bubble. At hypersonic speeds, as the base pressure is less than the pressure in the approach flow, the viscous shock layer expands around the shoulder, forming free shear layers that coalesce at the wake neck. A velocity profile defect characterizes the wake neck region, which continues downstream as the viscous wake region. A portion of the shear-layer flow must be recirculated to satisfy continuity requirements, thus producing a typical vortex pattern that is adjacent to the base. A complex in viscid wave structure often includes a lip shock (associated with the corner expansion) and a wake shock (adjacent to the shear-layer confluence). At very high Mach numbers, these wave patterns often interact with each other. Figure 8 shows that injecting small amounts of gas into the flow field behind the base of the projectile will split the originally large recirculation zone into three parts. One recirculation region remains at the symmetry axis and the other ones are formed right behind the base corner. As the mass flow rate increases, the recirculation zone at the axis is pushed further out and the other ones at the base corners become larger. If the mass flow rate is increased enough, the recirculation region near the axis disappears.[10, 26]

As shown in Fig. 8, the GMTI combustion products are more capable of transferring the heat released during injection in recirculation zone than the air. Presumably, this can be justified by the difference between the convective heat transfer coefficients average values (h).

### 3.3. The influence of propellant type

As stated above, in order to optimize the base bleed composition, some numerical computations on the axisymmetric geometry, have been performed in order to estimate drag force reduction using ANSYS-FLUENT$^{TM}$ software at a different supersonic Mach numbers (from 1,4 to 2,2), using RSM model, for jet-on conditions for all base bleed grains presented in Tab. 1. In addition, their effectiveness are compared with CO, $H_20$ and HCl injection at 1700 K.

Tab. 2, shows the CFD results at (M=2) for optimal injected impulse (mass flow rate), the base pressure ratio ($P_b/P_\infty$), the drag coefficient reduction and the critical impulse ($I_{critical}$) for the projectile

with base bleed combustion products injection. Additionally, the same parametres for CO, $H_2O$ and HCl are given.

**Table 2. Summary of the different results given in this study**

| Base bleed grain type (combustion temperature) | The average molar mass (g/mol) | $I_{optimal}$ | $p_b/p_\infty$ | $\Delta C_D$ % | $I_{critical}$ |
|---|---|---|---|---|---|
| GST_1 (2287K) | 21,349 | 0,0051 | 0,705 | 23,72 | 0,0052 |
| GST_2 (2050K) | 21,526 | 0,0064 | 0,682 | 23,03 | 0,0082 |
| GAL (2262K) | 22,797 | 0,0044 | 0,749 | 25,02 | 0,0055 |
| GHO (2442K) | 23,118 | 0,0051 | 0,746 | 24,92 | 0,0064 |
| GPVC (2587K) | 23,860 | 0,0056 | 0,817 | 26,85 | 0,0057 |
| CO (1700K) | ~ 28 | 0,0127 | 0,602 | 22,14 | 0,0153 |
| $H_2O$ (1700K) | ~ 18 | 0,0127 | 0,642 | 24,81 | 0,0129 |
| HCl (1700K) | ~ 36 | 0,0153 | 0,703 | 26,56 | 0,0205 |

According the Tab. 2, we can see the temperature effect on reducing the drag coefficient. The positive effect of the molecular weight of the injected combustion products can also be observed. Fig. 9 shows $\Delta C_D$ vs injected impulse (mass flow rate) CFD results at (M=2) for each propellant. Since the combustion temperatures interval from 2050K to 2587 K it can be concluded that the molecular weight has a significant role in terms of drag reduction. This was verified in [9, 27,28].

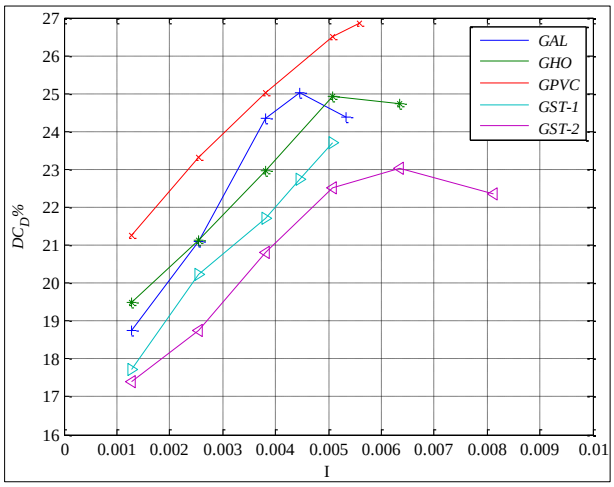


**Figure 9. CFD results at (M=2) for injected impulse (mass flow rate) vs $\Delta C_D$**

## 4. Conclusion

In order to estimate the influence of base bleed flow parameters on the drag force coefficient reduction ($\Delta C_D$), an axisymmetric 2D Reynolds Averaged Navier-Stokes (RANS) computational fluid dynamics (CFD) computations were performed at different values of the Mach numbers. The projectile calibre 122mm with base bleed (using different propellant types as base bleed grains) was studied. The modeled and grided (2-D) body geometry was exported to the software ANSYS-FLUENT$^{TM}$ to simulate

the airflow around the projectile for the zero angle of attack and Mach number range $0,9 \leq M \leq 2,2$ for projectiles with and without base flow injection.

The combustion products, which were obtained with the help of the thermochemical calculations, are introduced in the simulation. Additionally, in order to optimize the composition of base bleed grain, some preliminary simulations were performed using the RSM model, with injection of air, CO, $H_2O$ and HCl at different temperatures. The Supersonic/Initial Gauge Pressure was obtained from the static experimental combustion tests and used in the CFD calculations.

An experimental validation was made by following the projectile trajectory using the 3-D radar system model WEIBEL MFTR-2100.

The influence of the temperature effects on the drag coefficient is determined by CFD calculations. For the air injection, for the Mach number M = 2,2 the drag reduction ($\Delta C_D$ %) increase from ~7% at 300K to up to 18% at 2500K. Also, with the injection of GMTI combustion products when the temperature change from 1731K to 2500K, the drag coefficient reduction changes from 22% at 1731K to up to 26% at 2500K.

Also, according the CFD results for the projectiles with various propellant types, which the combustion temperatures change from 2050K to 2587 K (small interval) and seeing the CFD results with $H_2O$ and HCl injection (1700K), it can be affirmed that the molecular weight has an exceptional role in terms of drag reduction.

**References**


[1] Sahu, J., Supersonic flow over cylindrical afterbodies with base bleed, *Computational Mechanics*, *2* (1987) 3, pp.176-184. http://doi.org/10.1007/BF00571023

[2] Viswanath, P. R., Flow management techniques for base and afterbody drag reduction. *Progress in Aerospace Sciences*, *32* (1996), 2-3, pp. 79-129. http://doi.org/10.1016/0376-0421(95)00003-8

[3] Lee, Y., *Kim. H. -D.* , Optimization of mass bleed control for base drag reduction of supersonic flight bodies. *Journal of Thermal Science*, *15* (2006), 3, pp. 206-212. http://doi.org/10.1007/s11630-006-0206-4

[4] Mathur, T., Dutton, J. C, Base-bleed experiments with a cylindrical afterbody in supersonic flow, *Journal Of Spacecraft And Rockets*, *33* (1996), 1, pp. 30-37. http://dx.doi.org/10.2514/3.55703

[5] Andersson, K., *et al*., "Swedish Base Bleed" Increasing the range of artillery projectiles through base flow. *Propellants, Explosives, Pyrotechnics*, *1* (1976), 4, pp.69-73. http://dx.doi.org/10.1002/prep.19760010402

[6] Xue, X., Yu, Y., An improvement of the base bleed unit on base drag reduction and heat energy addition as well as mass addition. *Applied Thermal Engineering*, *109* (2016). pp. 238-250. http://dx.doi.org/10.1016/j.applthermaleng.2016.08.072

[7] Ding, Z., *et al*., Wind tunnel study of aerodynamic characteristics of base combustion. *Journal of Propulsion and Power*, *8* (1992), 3, pp. 630-634. http://dx.doi.org/10.2514/3.23525

[8] Hubbartt J E., *et al*., Mach 3 Hydrogen External/Base Burning. *AIAA Journal*, *19* (1981), 6, pp. 745-749. https://doi.org/10.2514/3.50998

[9] Bowman. J. E., Clayden, W. A., Cylindrical afterbodies at M sub infinity equals 2 with hot gas ejection. *AIAA Journal*, *6* (1968), 12, pp.2429-2431. http://dx.doi.org/10.2514/3.5009

[10] J. L. Herrin., Dutton, J. C., Supersonic Base Flow Experiments in the Near Wake of a Cylindrical Afterbody, *AIAA Journal*. *32* (1994), 1, pp. 77-83. http://dx.doi.org/10.2514/3.11953

[11] Przirembel, C. E., Valentine, D. T., Turbulent axisymmetric near-wake at Mach four with base injection. *AIAA Journal, 8* (1970), 12, pp. 2279-2280. https://doi.org/10.2514/3.6104

[12] Ansys Inc., ANSYS FLUENT 17.0 licensed to MA, 2017

[13] Regodić, D. *External Ballistic. (In Serbian language)*, Military Academy, Belgrade, Serbia, 2006.

[14] Tanner, M. Investigations into incompressible steady base flows. *Aerospace Science and Technology, 14* (2010), 2, pp. 126-133. http://dx.doi.org/10.1016/j.ast.2009.11.007

[15] Nicolás-Pérez, F *et al*. On the accuracy of RANS, DES & LES turbulence models for predicting drag reduction with Base Bleed technology. *Aerospace Science and Technology, 67* (2017),pp.126-140. https://doi.org/10.1016/j.ast.2017.03.031

[16] Novak, L., *et al*., Investigation of vortex shedding from an airfoil by CFD simulation and computer-aided flow visualization. *Thermal Science*,(2018)., pp. 1-12. https://doi.org/10.2298/TSCI170615002N

[17] Cvetinović, D., *et al*., Review of the research on the turbulence in the laboratory for thermal engineering and energy. *Thermal Science, 21* (2017), Suppl. 3, pp. S875-S898. https://doi.org/10.2298/TSCI160221330C

[18] Orlenko, P, L. *Physics of Explosion (Book in Russian language)*. FizMatLit, Moscow, Russia, 2002.

[19] Thunaipragasam, S., Natarajan, K. Experimental study on composite solid propellant material burning rate using matlab algorithm. *Thermal Science, 20* (2016), Suppl. 4, pp. S1119-S1125. https://doi.org/10.2298/TSCI16S4119T

[20] Jaramaz, S., Injac, M. Method of Calculation Range of Base Bleed Projectile. (In Serbian), *Military Technical Institute, Belgrade.* (1989).

[21] Jaramaz, S., Injac, M. Effect of Grain Characteristics on Range of Artillery Projectiles with Base Bleed, in: *First International Symposium on Special Topics in Chemical Propulsion,* Hemisphere Publishing Corporation, New York, USA, ISBN 0-89116-937-7, 1991, pp. 143-157.

[22] Zhang, L., *et al*., Burning rate of AP/HTPB base-bleed composite propellant under free ambient pressure. *Aerospace Science and Technology, 62* (2017), pp. 31-35. http://dx.doi.org/10.1016/j.ast.2016.12.004

[23] ***,Weibel Scientific Solvang, 2010, MFTR 2100 Medium Range TSPI & Debris Radar. Report ID CS-1017-006. Weibel Doppler Radars. Allerød Denmark. www.weibel.dk.

[24] Christopher J. F., The issue of numerical uncertainty, *Applied Mathematical Modelling, 26* (2002), 2, pp.237–248. http://dx.doi.org/10.1016/s0307-904x(01)00058-0

[25] Regodić, D., *et al*., The prediction of axial aerodynamic coefficient reduction using base bleed. *Aerospace Science and Technology, 31* (2013), 1, pp. 24-29. http://dx.doi.org/10.1016/j.ast.2013.09.001

[26] Sahu, J., *et al*.. Navier–Stokes Computations of Projectile Base Flow with and Without Mass Injection, *AIAA Journal, 23* (1985), 9, pp. 1348–1355. http://dx.doi.org/10.2514/3.9091

[27] Korkegi. R. H.,Freeman . L. M., Aft-body drag reduction by combined boat-tailing and base blowing at M sub infinity equals 3. *AIAA Journal, 14* (1976), 8, pp. 1143-1145. https://doi.org/10.2514/3.7206

[28] Tanner, M., Theoretical prediction of base pressure for steady base flow, *Progress in Aerospace Sciences, 14* (1973), pp. 177-225. http://dx.doi.org/10.1016/0376-0421(73)90006-7